Int. J. Heat Mass Transfer. Vol. 15, pp. 655–663. Pergamon Press 1972. Printed in Great Britain

BUBBLE GROWTH RATES DURING NUCLEATE BOILING AT HIGH JAKOB NUMBERS

JAMES K. STEWART* and ROBERT COLE
Department of Chemical Engineering, Clarkson College of Technology, Potsdam, New York 13676, U.S.A.

(*Received* 29 *April* 1971 *and in revised form* 6 *July* 1971)

Abstract—Bubble growth rates were investigated experimentally to determine further, the effect of high Jakob number conditions. Comparison of the experimental data with existing theory for Jakob numbers from 955 to 1112 show clearly that the discrepancies reported in earlier work [1] were primarily due to neglect of the effect of liquid inertia.

NOMENCLATURE

- A, bubble cross-sectional area;
- a, bubble width;
- a_{max} maximum bubble width;
- b_{max} maximum bubble height;
- q, heat flux;
- R_{eq}, equivalent radius of a bubble;
- t_w, waiting time between successive bubbles;
- T_0, bulk temperature of liquid;
- T_{sat}, saturation temperature of liquid at the boiling surface;
- T_w, wall temperature;
- ΔT, wall superheat $= T_w - T_{sat}$;
- V, bubble volume.

INTRODUCTION

IN A PREVIOUS paper, Cole and Shulman [1] presented an experimental study of bubble growth rates to determine whether bubble growth theories advanced to that date (all of which had neglected dynamic or inertial effects as being unimportant after the first few microseconds) reasonably described the growth process from a solid surface at high Jakob numbers. The results of that study revealed discrepancies of such magnitude that a reexamination of the theory was recommended, with emphasis on determining the relative importance of dynamic effects.

Three factors however seemed to detract from the experimental results:

1. The bubbles grew to such a large size that their shape was influenced by the geometry of the heating surface (a 12·7 mm wide × 100 mm long × 0·254 mm thick zirconium ribbon).
2. The volume average ribbon temperature (as determined by resistance thermometry) was not sufficiently accurate and as a result, the maximum possible error in the superheat measurement was felt to be excessive (50 per cent).
3. Only three bubbles were obtained at the highest Jakob number (792).

The objective of the present work was to obtain additional bubble growth data at high Jakob numbers with an experimental system improved to enable more accurate superheat measurements and to eliminate the effect of geometry upon bubble shape.

EXPERIMENTAL APPARATUS AND PROCEDURE

The system, illustrated in Fig. 1 consisted of a cylindrical aluminium tank fitted with four fused silica glass windows. Passing through the top of the tank are a vacuum line, two bulk

* Present address: Proctor and Gamble Co., Cincinnati, Ohio.

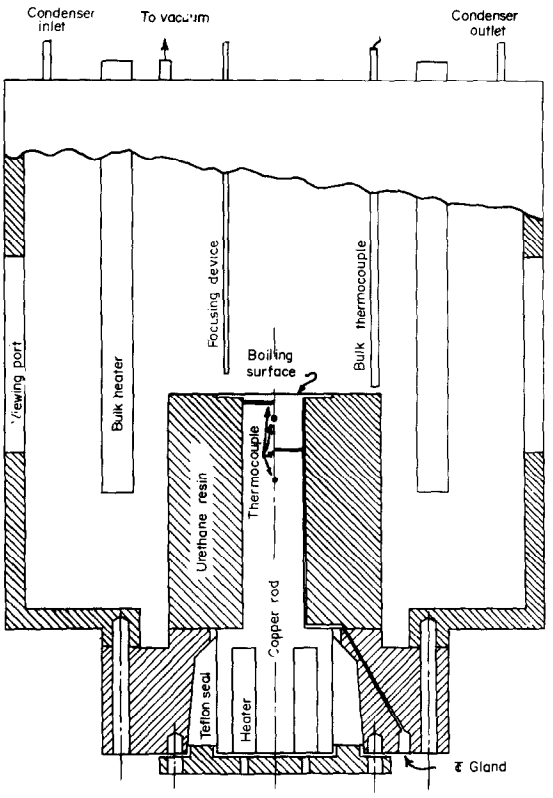

FIG. 1. Diagram of boiling apparatus.

immersion heaters, a stainless steel sheathed thermocouple, inlet and outlet for the water cooled internal condenser, and a focusing device. Sub-atmospheric pressures were obtained by means of a vacuum pump and measured with a U-tube manometer.

The boiling surface was the top face of a long copper rod. An integral thin circular fin was formed on this face by machining a length of the rod to a diameter of 25·4 mm. Thus, although the diameter of the top face of the rod was 44·5 mm, a portion of this was fin surface (for the purpose of minimizing unwanted edge nucleation) and the boiling surface diameter was taken to be 25·4 mm. In order to minimize radial heat losses to the surrounding water, the copper rod was insulated around its periphery by a thick layer of clear Urethane resin, polymerized in place, with outside diameter 82·5 mm. The heat source consisted of four 200 W cartridge heaters embedded in the base of the copper rod.

For the purpose of determining the boiling surface temperature and the heat flux, the temperatures within the copper rod were measured at four different axial locations. Four copper–constantan thermocouples, doubly insulated with "Teflon", were located in wells precisely drilled to the center of the copper rod, at known distances from the boiling surface. After insertion of the thermocouples, the wells were sealed with a thermosetting type synthetic resin which bonds "Teflon" to metal and which maintains its adhesive strength to 150°C.

In an attempt to reduce the experimental superheat measurement error, differential temperature measurements were made; the readings of the four rod thermocouples being taken relative to that of the bulk thermocouple. The differential output was fed to a multipoint millivolt recorder so that a time record is available for each run. By using a switch box, the bulk liquid thermocouple was read separately (relative to the ice point) using a millivolt potentiometer.

The boiling surface was polished to a mirror-like finish using standard metallurgical polishing techniques. Final polishes were applied with polishing cloths and 15 and 5 μ alumina slurry.

Prior to insulating the heating rod, the rod thermocouples were calibrated in place (after being sealed into the rod thermocouple wells) relative to the bulk liquid thermocouple. Two constant temperature baths were used for this purpose. The bulk liquid thermocouple was placed in a bath whose temperature was maintained at 35°C using an immersion heater, a thermoregulator, and a motor driven stirrer. The 35°C temperature was the approximate saturation temperature for the pressure at which the runs were to be made. The copper rod with the embedded thermocouples was immersed in a second tank of water kept at a different constant temperature. The actual water temperature in each bath was measured using

the same U.S. National Bureau of Standards calibrated thermometer. The system was allowed to reach steady tate and the e.m.f. difference recorded using the multipoint millivolt recorder. The procedure was repeated for different temperatures of the copper rod at intervals of 5°C from 35°C to 70°C, yielding a calibration graph of ΔT vs. e.m.f. for each of the four thermocouples. The bulk liquid thermocouple was calibrated separately at various temperatures relative to the ice point.

All the runs were conducted with water as the boiling medium. A moderate vacuum was applied and the voltage to the bulk heaters regulated so as to allow the water to reach the saturation temperature. Tap water was allowed to flow through the condenser and the voltage to the cartridge heaters in the copper rod adjusted to obtain the desired degree of boiling. The recorder was turned on and the absolute temperature of the bulk liquid was measured using the potentiometer. The system was allowed to operate a minimum of six hours to insure that steady state conditions had been attained.

A "Fastax" high speed motion picture camera with 50 mm, f/2 lens was used to record the boiling action and was focused over the heating surface with the aid of the reference device. The lamp used for illumination was a single 750 W pre-focused reflector type, placed behind the viewing port opposite the camera. One thousand cycle/s timing marks were recorded on the film by means of a timing light generator and a neon timing lamp within the camera. The camera was operated at a speed of 3000 frames/s and the film (16 mm half width) developed to a positive image using a reversal process.

METHODS OF MEASUREMENT AND CALCULATION

In order to obtain quantitative information on the dynamics of the bubble motion, the film was analyzed frame by frame using a Vanguard Motion Analyzer which supplied a 15× magnification of film size to viewed image. A typical bubble growth tracing is shown in Fig. 2.

In this work, the bubbles formed near the center of the heating surface and grew in a symmetrical manner, i.e. the bubble profiles shown in Fig. 2 can be considered as surfaces of revolution about the vertical axis to form the shape and volume of the bubble. Such behavior was verified experimentally by employing two high speed cameras operating simultaneously in such a fashion that the bubbles were photographed from two directions, $\pi/2$ radians apart. Growth rates obtained from such films are illustrated for a typical bubble in Fig. 3. In all instances where this technique was employed, the difference in the two curves was less than the estimated experimental error. Consequently, the procedure was eliminated as unnecessary.

In [1], it was shown that the method of determining bubble diameters or radii was not critical in its effect upon the bubble growth curve. In this work, the bubble volume was first computed for the bubble in Fig. 16 ($t_w = 863$ ms) using Simpson's rule for irregular volumes [2, 3]. In essence, the bubble profile is divided into $2m + 1$ parallel lines, a distance h apart to yield $2m$ circular discs. Then by Simpson's rule, the volume is given by

$$V = \tfrac{1}{3}h[(A_0 + A_{2m}) + 4(A_1 + A_3 + \ldots + A_{2m-1}) + 2(A_2 + A_4 + \ldots + A_{2m-2})] \quad (1)$$

where $A_i = \pi a_i^2/4, \quad i = 0, 1, 2, \ldots$

An equivalent radius may then be computed as the radius of a sphere having the same volume as the bubble. The radius–time curve computed using this time consuming procedure is compared in Fig. 4 with the radius–time curve computed from the simple relation

$$R_{eq} = \frac{a_{max} + b_{max}}{4} \quad (2)$$

where the dimensions a_{max} and b_{max} are defined on Fig. 2.

It is apparent that there is little difference between the two results. Consequently bubble radii were computed for this work from equation (2).

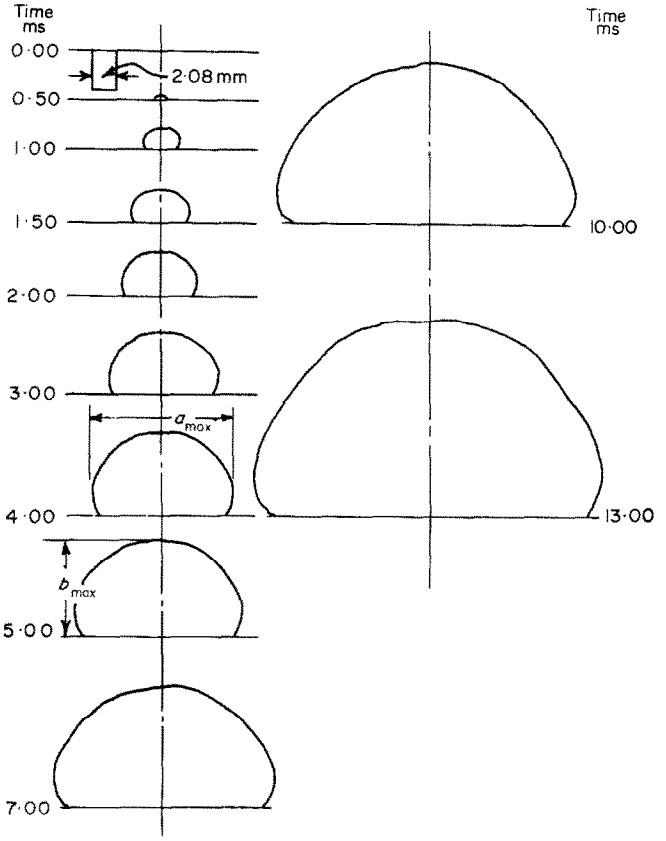

FIG. 2. Bubble growth tracings for Fig. 16 (t_w = 863 ms).

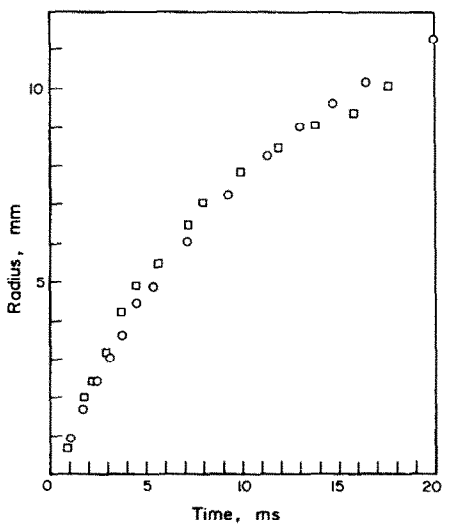

FIG. 3. Bubble growth data obtained by means of two cameras operating simultaneously from directions $\pi/2$ radians apart.

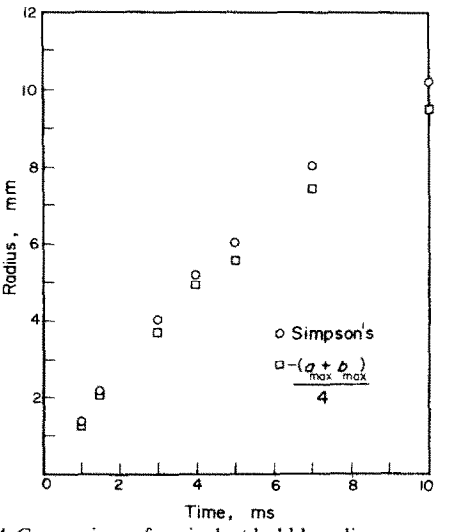

FIG. 4. Comparison of equivalent bubble radius as computed by Simpson's rule and by equation (2).

The temperatures of the four rod thermocouples relative to that of the bulk are determined from the voltages recorded and the calibration curve. To compute this temperature difference at the heating surface, the method of least squares was used in preference to graphical extrapolation. A linear axial temperature profile in the copper rod, with uniform radial distribution, was assumed. The least square method also directly provided the temperature gradient in the copper rod which was used to compute the heat flux from the boiling surface. The experimental rod temperatures (corresponding to the growth data shown in Fig. 15) along with the least square extrapolation to the surface is shown in Fig. 5.

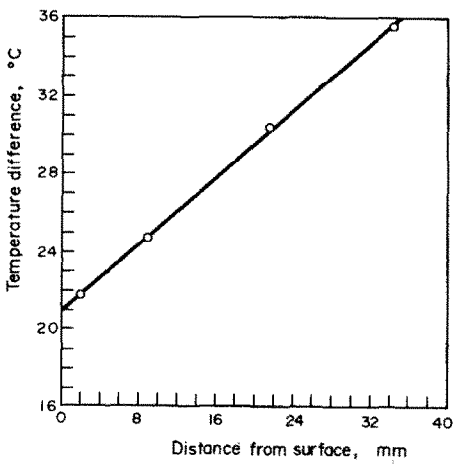

FIG. 5. Temperature profile in copper rod.

The maximum error in the temperature difference between the rod thermocouples and the bulk liquid was estimated to be 0·71°C. There was further possible error in the extrapolation of these temperature differences to determine the surface temperature difference. This is estimated from curves such as Fig. 5 to be 0·8°C. The possible error in the measurement of the surface temperature relative to the bulk was thus estimated as 1·52°C. For a typical run, this represents a maximum possible error of 7·6 per cent in the difference $(T_w - T_0)$. The possible error associated with the absolute temperature of the bulk liquid (measured separately) was 0·43°C and represents a maximum possible error of 1·3 per cent in T_0. Fluctuations of ± 6 mm of Hg were observed from the mercury manometer. Assuming this to represent the possible error in system pressure, the corresponding error in the saturation temperature of the liquid is 2·5°C. This represents a maximum possible error of 7·7 per cent in T_{sat}. The wall superheat ΔT defined as $T_w - T_{sat}$ must be computed from the expression:

$$(T_w - T_{sat}) = (T_w - T_0) + (T_0 - T_{sat}) \quad (3)$$

since the bulk liquid was apparently superheated rather than being at the saturation temperature. Thus, the error in this superheat is additive and amounts to a maximum possible error of 21·2 per cent, the greatest contribution being due to the possible error in T_{sat}.

RESULTS AND DISCUSSION

The experiments were conducted at a pressure of 4·9 kN/m^2 with the wall superheat $(T_w - T_{sat})$ ranging from 19·35 to 22·54°C, correspond-

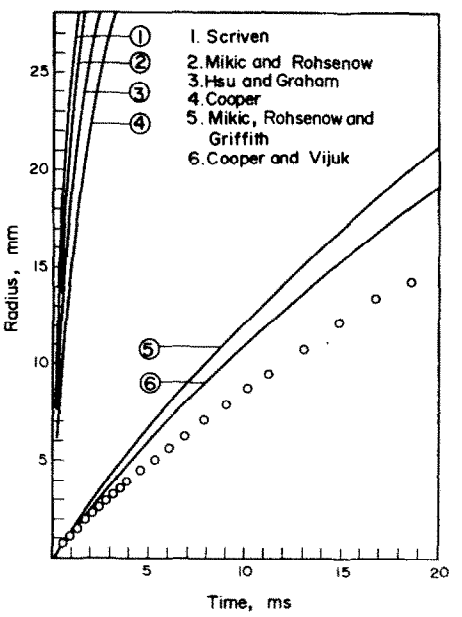

FIG. 6. Comparison of bubble growth models with data, $P = 4{\cdot}9$ kN/m^2, $T_w - T_{sat} = 21{\cdot}3$ degC, $T_w - T_0 = 20{\cdot}2$ deg C, $N_{Ja} = 1051$, $q = 1{\cdot}71 \times 10^5$ W/m^2.

ing to Jakob numbers from 955 to 1112, respectively. The bubble radii are plotted in Figs. 6–16 as a function of time for each of the bubbles analyzed. In these figures, the ordinate has been limited to 12 mm because bubbles having radii exceeding this value by a slight amount would be extending onto the fin area of the test surface. Thus, it should be recognized that the data presented represents only a small portion (perhaps 25 per cent) of the total growth period.

Figure 6 is presented to show that the data again indicate order of magnitude discrepancies between experiment and the diffusion controlled models, regardless of whether they are of the

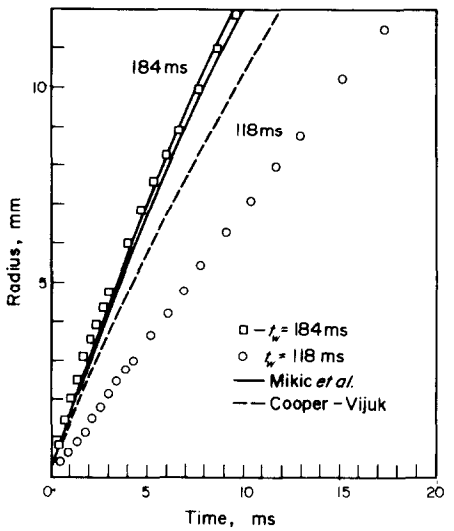

FIG. 7. Bubble growth data, $P = 4{\cdot}9$ kN/m^2, $T_w - T_{sat} = 20{\cdot}1$ degC, $T_w - T_0 = 19{\cdot}1$ degC, $N_{Ja} = 993$, $q = 1{\cdot}71 \times 10^5$ W/m^2.

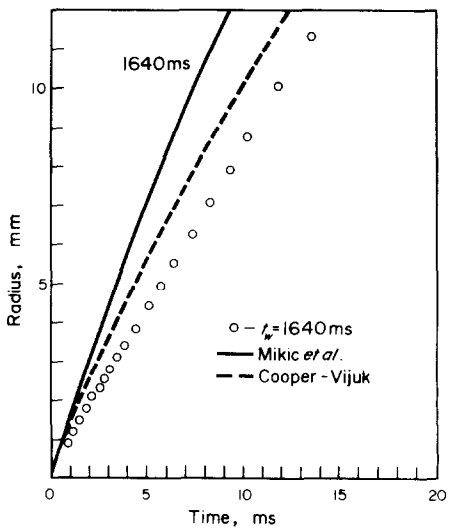

FIG. 9. Bubble growth data, $P = 4{\cdot}9$ kN/m^2, $T_w - T_{sat} = 19{\cdot}4$ degC, $T_w - T_0 = 18{\cdot}3$ degC, $N_{Ja} = 955$, $q = 1{\cdot}79 \times 10^5$ W/m^2.

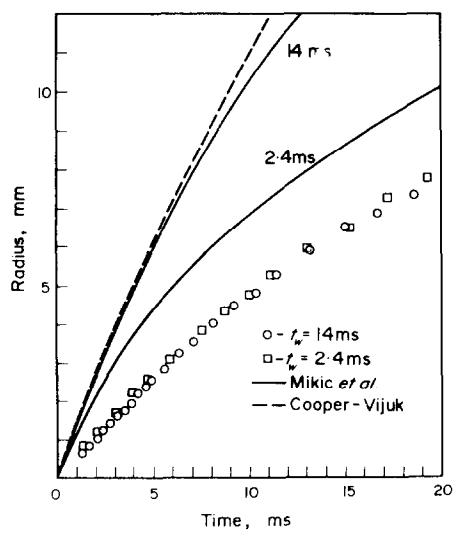

FIG. 8. Bubble growth data, $P = 4{\cdot}9$ kN/m^2, $T_w - T_{sat} = 21{\cdot}5$ degC, $T_w - T_0 = 20{\cdot}5$ degC, $N_{Ja} = 1062$, $q = 1{\cdot}52 \times 10^5$ W/m^2.

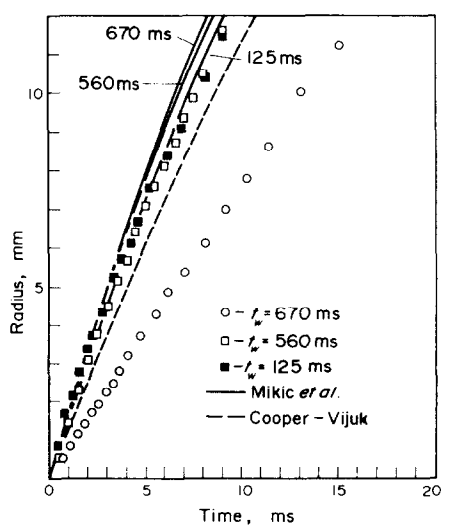

FIG. 10. Bubble growth data, $P = 4{\cdot}9$ kN/m^2, $T_w - T_{sat} = 22{\cdot}5$ degC, $T_w - T_0 = 21{\cdot}5$ degC, $N_{Ja} = 1112$, $q = 1{\cdot}51 \times 10^5$ W/m^2.

uniform superheat [4], non-uniform superheat [5, 6] or microlayer type [7]. Two models [8, 9] however, which include the effect of liquid inertia are in much closer agreement with the data. Interestingly, one of these [9] is of the microlayer type, while the other [8] is an extension of the analysis presented in [5].

In Figs. 7–16, the experimental growth data are compared with the numerical solution of equation (17) of the analysis of Mikic, Rohsenow and Griffith [8] and equation (26) of Cooper and Vijuk [9]. Since the latter analysis assumes a hemispherical bubble, their analytical expression for the bubble radius has been multiplied

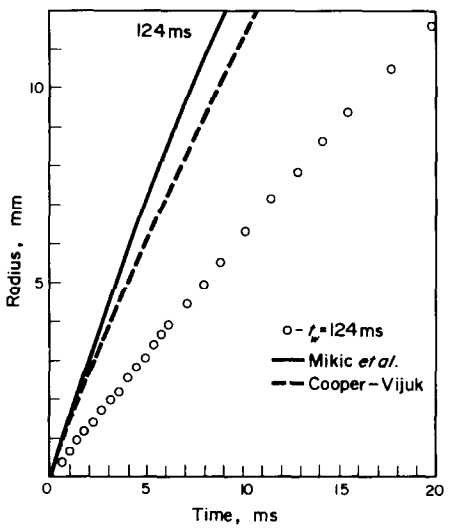

FIG. 11. Bubble growth data, $P = 4{\cdot}9$ kN/m^2, $T_w - T_{sat} = 22{\cdot}1$ degC, $T_w - T_0 = 21$ degC, $N_{Ja} = 1089$, $q = 1{\cdot}66 \times 10^5$ W/m^2.

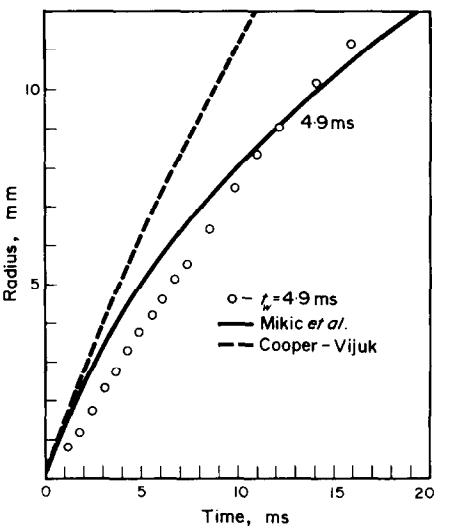

FIG. 13. Bubble growth data, $P = 4{\cdot}9$ kN/m^2, $T_w - T_{sat} = 22{\cdot}3$ degC, $T_w - T_0 = 21{\cdot}3$ degC, $N_{Ja} = 1101$, $q = 1{\cdot}65 \times 10^5$ W/m^2.

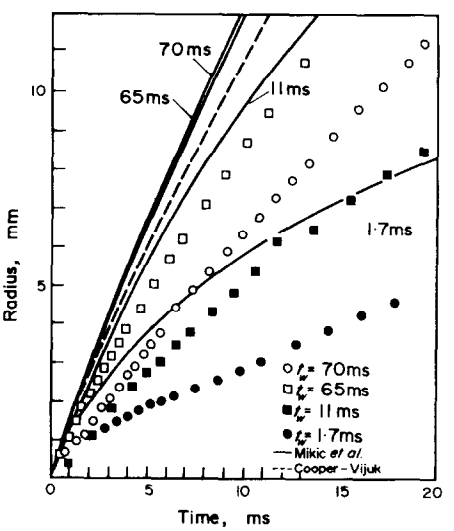

FIG. 12. Bubble growth data, $P = 4{\cdot}9$ kN/m^2, $T_w - T_{sat} = 21{\cdot}3$ degC, $T_w - T_0 = 20{\cdot}2$ degC, $N_{Ja} = 1051$, $q = 1{\cdot}71 \times 10^5$ W/m^2.

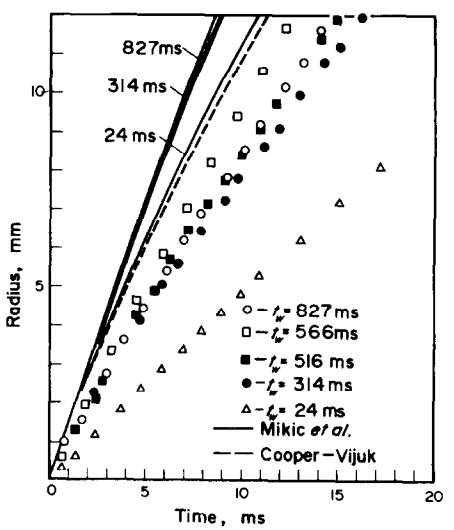

FIG. 14. Bubble growth data, $P = 4{\cdot}9$ kN/m^2, $T_w - T_{sat} = 21{\cdot}7$ degC, $T_w - T_0 = 20{\cdot}7$ degC, $N_{Ja} = 1071$, $q = 1{\cdot}66 \times 10^5$ W/m^2.

by $(\frac{1}{2})^{\frac{1}{3}}$ to give the radius of a sphere having the same volume as a hemisphere. It should be emphasized that this has been done only to facilitate comparison of the experimental data with both analyses. In general, the comparison

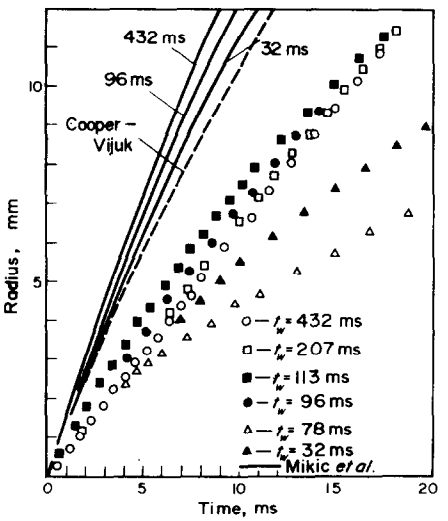

FIG. 15. Bubble growth data, $P = 4{\cdot}9$ kN/m^2, $T_w - T_{sat} = 20{\cdot}8$ degC, $T_w - T_0 = 19{\cdot}7$ degC, $N_{Ja} = 1024$, $q = 1{\cdot}71 \times 10^5$ W/m^2.

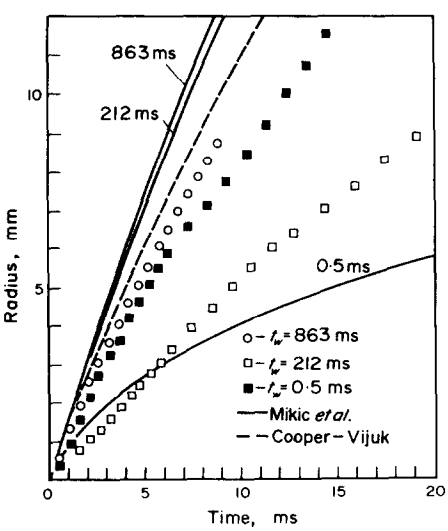

FIG. 16. Bubble growth data, $P = 4{\cdot}9$ kN/m^2, $T_w - T_{sat} = 22{\cdot}0$ degC, $T_w - T_0 = 20{\cdot}9$ degC, $N_{Ja} = 1084$, $q = 1{\cdot}68 \times 10^5$ W/m^2.

seems to leave little doubt that the major discrepancies observed in previous work were indeed due to the neglect of the effect of liquid inertia.

Figure 17 is a plot of the various pressure terms in the extended Rayleigh equation as obtained by graphical differentiation of the experimental data for the bubble in Fig. 12 having a waiting period of 11 ms. The liquid inertia term is seen to be greater than the surface tension term by a factor of 30 over the measured period of observation. The bubble should thus tend towards a hemispherical shape having significant contact area with the heating surface

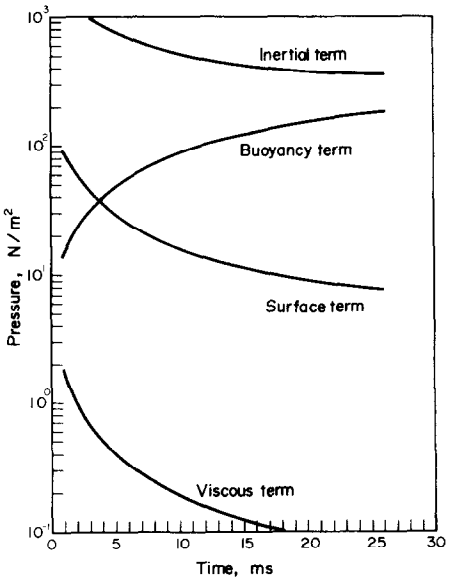

FIG. 17. Pressure terms in the extended Rayleigh equation.

(as shown in Fig. 2). Under such conditions microlayer evaporation rather than vaporization around the curved surface of the bubble would be expected to be the predominant mechanism for bubble growth. Yet, in Figs. 7–16, it is not possible to conclude that the microlayer analysis of Cooper and Vijuk is in better agreement with the data than is the analysis of Mikic, Rohsenow and Griffith. Further, neither analysis yields agreement which could be considered

quite satisfactory. For example, the Cooper–Vijuk analysis assumes uniform superheat in the microlayer and thus requires an asymptotic solution (i.e. infinite waiting period). A glance at Figs. 7–16 shows quite clearly that the analysis is in reasonable agreement with the data only at large values of the waiting period. The Mikic–Rohsenow–Griffith model, although not asymptotic, almost consistently overestimates the growth rate. Whether this is due to the model being in error, or to other causes such as integrating from zero radius while neglecting surface tension forces, is not known. Additionally the experimental data do not confirm the predicted variation of growth rate with waiting time; discrepancies existing in most of the figures.

Nevertheless, it is quite apparent from Fig. 6 that liquid inertia is a major factor restricting the rate of growth of vapor bubbles at low pressures, and that models which include this effect are at least of the proper order of magnitude. Whether other factors such as the kinetic resistance at the interface are additionally important will probably not be determined until present analyses are further refined.

ACKNOWLEDGEMENTS

The authors are grateful for support given by the National Science Foundation through Grant Number GK-863. Mr. Padmanabha J. Prabhu performed the frame by frame analysis of the high speed film.

REFERENCES

1. R. Cole and H. L. Shulman, Bubble growth rates at high Jakob numbers, *Int. J. Heat Mass Transfer* **9**, 1377 (1966).
2. *C.R.C. Standard Mathematical Tables*, edited by C. D. Hodgman, 12th edition, p. 402. Chemical Rubber Publishing Company, Cleveland (1962).
3. K. L. Nielsen, *Methods in Numerical Analysis*, p. 119. Macmillian, New York (1956).
4. L. E. Scriven, On the dynamics of phase growth, *Chem. Engng Sci.* **10**, 1 (1959).
5. B. B. Mikic and W. M. Rohsenow, Bubble growth rates in non-uniform temperature field, *Progress in Heat and Mass Transfer II*, p. 283. Pergamon, Oxford (1969).
6. Y. Y. Hsu and R. W. Graham, An analytical and experimental study of the thermal boundary layer and ebullition cycle in nucleate boiling, NASA TN D-594 (May 1961).
7. M. G. Cooper, The microlayer and bubble growth in nucleate pool boiling, *Int. J. Heat Mass Transfer* **12**, 915 (1969).
8. B. B. Mikic, W. M. Rohsenow and P. Griffith, On bubble growth rates, *Int. J. Heat Mass Transfer* **13**, 657 (1970).
9. M. G. Cooper and R. M. Vijuk, Bubble growth in nucleate pool boiling, *Proceedings of the 4th International Heat Transfer Conference*, Paris–Versailles, V. B 2.1 (1970).

VITESSES DE CROISSANCE D'UNE BULLE LORS D'UNE ÉBULLITION NUCLÉÉE POUR DES NOMBRES DE JAKOB ÉLEVÉS

Résumé—Des vitesses de croissance d'une bulle ont été obtenues expérimentalement pour déterminer ultérieurement l'effet des grands nombres de Jakob. Une comparaison des résultats expérimentaux avec la théorie déjà existante pour des nombres de Jakob compris entre 955 et 1112 montre clairement que les désaccords rapportés dans un travail antérieur sont dus principalement au fait que l'on néglige l'effet d'inertie du liquide.

BLASENWACHSTUM WÄHREND DES BLASENSIEDENS BEI HOHEN JAKOB-ZAHLEN

Zusammenfassung—Blasenwachstumsraten wurden experimentell untersucht, um den Einfluss der Bedingungen bei hohen Jakob-Zahlen zu bestimmen. Der Vergleich von Versuchsdaten mit der bestehenden Theorie für Jakob-Zahlen von 955 bis 1112 zeigt klar, dass die Diskrepanzen, die in früheren Arbeiten [1] auftraten, vor allem der Vernachlässigung des Einflusses der Flüssigkeitsmassenkräfte zuzuschreiben waren.

СКОРОСТИ РОСТА ПУЗЫРЬКОВ ПРИ ПУЗЫРЬКОВОМ КИПЕНИИ ПРИ БОЛЬШИХ ЧИСЛАХ ДЖЕКОБА

Аннотация—Экспериментально исследовались скорости роста пузырьков, чтобы определить влияние больших чисел Джекоба. Сравнение экспериментальных данных с существующей теорией для чисел Джекоба от 955 до 1112 ясно показывает, что различия, о которых писалось ранее [1], в основном, объясняются пренебрежением влияния инерции жидкости.